1

Basics of Neuromagnetism and Magnetic Source Imaging

Lloyd Kaufman
New York University

Zhong-Lin Lu
University of Southern California

This chapter is for both the sophisticated researcher and also for students and nonspecialists. It provides the groundwork needed to understand *magnetic source imaging* (MSI) with an intuitive account of the science of *neuromagnetism*. This includes the neurogenesis of the brain's magnetic field and also the technology needed to detect such exquisitely weak magnetic fields. Methods for discriminating against ambient magnetic fields (noise) are also discussed. We describe how to map the extra cranial field about the head and what might be deduced from such maps. Frequently, the source of an observed field is assumed to be an *equivalent current dipole* (ECD), which may be thought of as a "center of gravity" of an extended region of cerebral cortex. Field maps are used in locating ECDs within the skull. However, this also requires an explicit model of the head (e.g., a sphere that best fits the region of skull over which fields are measured). We describe the possibility for going beyond the ECD to define the actual source distribution. In principle, this so-called *inverse problem* has no unique solution. However, when properly constrained (e.g., using knowledge of cortical geometry), it may be possible to achieve unique solutions to some inverse problems. We also take up so-called spontaneous brain activity. We make the point that the meaning of concepts such as *desynchronization* can only be understood by explicitly taking the geometry of the brain

into account. Also, the duration of localized changes in spontaneous activity corresponds accurately to behavioral measures of time-varying cognitive processes such as mental rotation and searching short-term memory. Furthermore, we discuss the interaction (cross-modulation) of spontaneous and event related brain activity, which is seen as a necessary consequence of the intrinsic nonlinearity of the brain. We make clear a major implication of this insight, namely, the so-called noise discarded in normal signal averaging may well contain information vital to understanding how the brain reacts to stimuli and how it goes about the processes involved in cognition. We also discuss how event-related activity originating in different neural pathways might also interact with each other. Such interaction and its absence may be used as a tool signifying whether different channels are or are not independent of each other, a distinction vital to some theories of how the nervous system is organized. Finally, we briefly describe complementary functional imaging modalities such as PET and fMRI, and compare these with MSI and EEG. The relationship between EEG and MSI is discussed throughout the chapter, and this may well be of value to specialists in EEG and the classic event-related potential. Finally, we mention some clinical applications of MSI. Throughout the chapter we cite other chapters on this volume that treat many of the topic considered at a more detailed and advanced level.

This chapter provides an overview of *neuromagnetism,* which is defined as the study of magnetic fields associated with the electrical activity of neurons. Like the other chapters in this volume, this chapter especially emphasizes the magnetic fields generated by the human brain. In view of this emphasis, we introduce the reader to *magnetoencephalography*, a technique that measures the external magnetic field, near the scalp, of the intact human brain. This general overview is designed to help newcomers appreciate the more technical chapters. It provides a relatively nontechnical description of the physical basis of the neuromagnetic field, the different methods used to detect it, and how the magnetoencephalogram complements the *electroencephalogram*. We explain how analysis of MEG data can yield high temporal and reasonable spatial resolution "representations" of current distributions on the cerebral cortex. These magnetic source images complement the other functional imaging modalities. Furthermore, we describe some typical uses of *magnetic source imaging* in medicine and in cognitive neural science. Finally, we briefly discuss complementary modes of functional brain imaging, such as *positron emission tomography* and *functional magnetic resonance imaging*, as well as recent attempts to combine multiple imaging modalities to achieve high spatiotemporal resolution functional images of the human brain. One goal of this chapter is to acquaint readers with areas of research that are awaiting the attention of creative scientists. To achieve this

goal, we must make a seemingly esoteric subject accessible. Hence, this chapter does not provide an exhaustive review of the literature; instead, we attempt to elucidate relevant principles, methods, and results in as simple a manner as possible and point the way so that even beginners will recognize opportunities to make advances in the field. The other chapters in this volume cite the relevant literature and describe historical precedents in great detail and can serve as a basis for further study and research. Thus, one of our major goals is to prepare beginners to read these chapters.

THE NEUROGENESIS OF MAGNETOENCEPHALOGRAPHY

In chapter 2 of this volume, Yoshio Okada provides a detailed discussion of how neurons give rise to magnetic fields. In this section we offer a brief and simplified account.

Primary and Volume Currents

Neurotransmitters crossing a synapse produce local changes in the electric potential across the target membrane. This postsynaptic potential tends to be either excitatory or inhibitory; that is, it either reduces or increases the polarization of the target membrane, depending on the nature of the neurotransmitter. The interior resting voltage of the cell is normally negative with respect to its exterior. As the polarization of the membrane is reduced, or even reversed, near the synapse the internal potential of the cell membrane becomes less negative relative to that of more distant regions of the membrane. This difference in potential between one region of the cell's inner wall and that of more distant regions results in current flow. Conversely, when the local transmembrane potential is increased (hyperpolarized) so that negativity of the interior of the membrane is greater near the synapse relative to more distant regions, negative ions will tend to flow away from that region toward more distant portions of the cell. This intracellular ionic current flow may persist for a relatively long time. The entire neuron can be thought of as a very small battery and a resistor connected to its positive pole. The battery–resistor combination is immersed in a saline solution. Because the solution is a conductor, it completes the circuit between the (positive) end of the resistor and the negative pole of the battery. This allows ionic current to flow widely throughout the solution from the positive end of the resistor to the opposite (negative) pole of the battery. The positive end of the resistor tends to lose charge as negative ions flow from it into the saline medium. This charge is replaced by ions from within the battery. These negative ions inside the battery are replen-

ished in turn by inflowing ions from the medium. As a consequence, charge is conserved, because there is a continuous flow of current around the complete battery–resistor–medium circuit. We refer to the intracellular current, within the battery and resistor, as the *primary current.* The primary current represents the ionic currents flowing within elongated processes of neurons, for example, dendrites of pyramidal cells of the cerebral cortex. Alternatively, the currents flowing outward from the battery–resistor circuit into the saline solution and inward from that solution toward the circuit's opposite pole are referred to as the *volume currents.* These currents correspond to extracellular currents that flow within the cerebrospinal fluid throughout the intracranial space. Because the skull has very high electric resistance, volume currents flow through the orbits of the eyes and other openings in the skull into the scalp, where they create the potential differences that underlie the electroencephalogram (EEG). The magnetic fields surrounding the neurons pass undisturbed through the skull to produce the magnetoencephalogram (MEG).

Both the volume currents and the intracellular ionic currents are depicted schematically in Fig. 1.1. In this instance, we assume that the source of the magnetic field **B** is a segment of current that is very small relative to the distance at which the field is measured. Hence, it is possi-

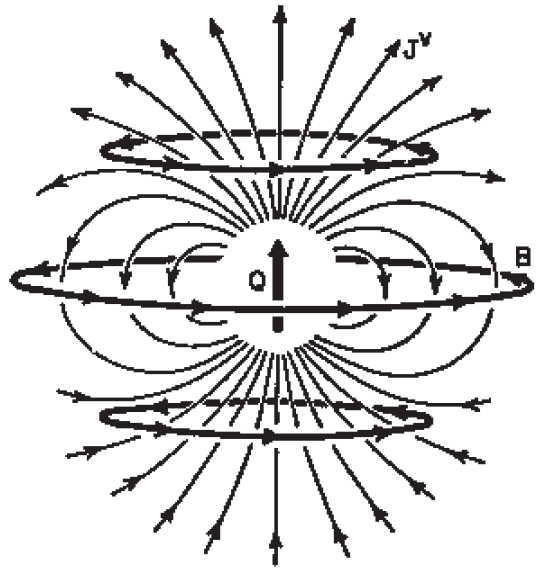

FIG. 1.1. A current dipole immersed in a homogeneous conducting medium. The magnetic field (**B**) is due solely to the current dipole (moment = Q), with the volume currents (represented by the thin lines [J^v]) making no contribution to the field.

ble to model it as an *equivalent current dipole* (ECD). Because magnetic fields are superimposable (i.e., they are additive and do not interact with each other), extracranial fields do not arise from a single neuron but actually represent the sum of the fields of many similarly oriented hypercolumns of concurrently active cortical cells.

In Fig. 1.1, $\mathbf{Q} = I \times \vec{L}$, where I is the amplitude of the current and $\vec{L}$ is the length and direction of the current segment. Because the dipole has both direction and strength, $\mathbf{Q}$ is a vector quantity representing the strength of the dipole in ampere–meters (the dipole's *moment*). The volume current also varies in strength and direction. The symbol $\mathbf{J}^{\mathbf{V}}$ indicates that the value of the direction and strength of the volume current depends on the position at which it is measured.

All moving electric charges are accompanied by magnetic fields. Because the volume currents are composed of moving electric charges, these too must be accompanied by magnetic fields. However, when the dipole is immersed in an infinitely large volume (or in a finite sphere), the direction of the field associated with an ion at one place and time is opposite from that associated with ions at other places at the same time. Therefore, the fields of these oppositely directed moving charges cancel each other out, that is, the sum of the fields of the volume current measured at some distant point is effectively zero. Thus, the field measured at a distance is due solely to the net primary current, which is largely associated with postsynaptic dendritic potential changes.

A distinction is often made between *open-field* and *closed-field* neurons. The latter are so designated because their dendritic trees are approximately symmetrical in three dimensions. Because of their morphological symmetry, these cells are presumed to contribute little to either electric or magnetic fields detected some distance away, because the net electric and magnetic fields produced by symmetric current distributions are zero. For example, basket cells are sometimes described as closed-field cells. On the other hand, pyramidal cells are prototypical open-field neurons, because their apical dendrites incorporate one-dimensional elongated processes. Ionic currents within these dendrites are excellent candidate sources of external fields and potentials. However, one must bear in mind that cell morphology alone does not determine whether a cell's magnetic field is detectable at a distance. For a cell with a symmetric dendritic tree, there could still be an asymmetric distribution of primary current (e.g., due to asymmetric presynaptic activities) and therefore a field that can be detected at a distance. Thus, although the literature often implies that pyramidal cells are the sole sources of external fields, this claim has not been

proved. For example, stellate cells do not have elongated dendrites. They, and not pyramidal cells, are predominant in the visual cortex. Yet some of the strongest MEG (and EEG) signals arise from the visual cortex.

As already noted, the volume currents flowing in the dermis of the scalp create the potential differences that underlie the EEG. Brain tissue and the fluid filling the subarachnoid space are relatively good conductors, especially as compared with the skull, which is highly resistive. These anisotropies in conductivity must be taken into account in attempts to identify the neural sources of scalp-detected potentials (Nunez, 1981). The difficulties in locating neural sources of EEG/event-related potential (ERP) are further compounded by the fact that the skull and other tissues are relatively asymmetrical, so that the paths of flowing volume currents are also asymmetrical. Finally, in measuring the EEG (as well as the ERPs considered later), one must use a reference or ground electrode. This is never a truly indifferent electrode, as it is affected by activity of the brain at regions that may be far from the "active" electrode. One must take this into account in interpreting a pattern of potentials across the scalp. Despite these factors, the EEG is capable of providing vital information regarding the linkage between particular scalp-detected phenomena and underlying process. For example, the presence of the classic spike and wave in the EEG may be diagnostic of epilepsy, even though sometimes it is not possible to accurately determine the location of the lesion responsible for seizures. To take another example, despite early controversy regarding the source of the N100 component of the *auditory-evoked potential* (AEP), this component proved to be a useful candidate for the study of attention.

To summarize, the scalp is "transparent" to magnetic fields (see chap. 2, this volume) but not to the electric potential produced by the brain. This makes interpretation of MEG a much simpler problem than that of EEG. Even though many recent ERP localization methods attempt to take account of these conductivity problems by using sophisticated volume conductor models of the head, ERP source localization is still a very difficult problem. A good example is in the study of N100, a relatively negative voltage peak (component) in the AEP that occurs about 100 msec after the onset of an acoustic stimulus. (In the MEG literature, the magnetic counterpart to N100 is often referred to as *M100*.) The AEP is normally detected at a midline electrode (at the vertex). As explained in chapter 9 of this volume, the sources of this component lie within the auditory cortex of each of two hemispheres. MEG experiments have revealed that at least two (and probably more) sources in each hemisphere underlie N100. The sources in the two hemispheres differ in strength and are affected somewhat differently by at-

tention to tonal stimuli (Curtis, Kaufman, & Williamson, 1988). The many published AEP studies do not report this asymmetry. Similarly, auditory evoked fields (AEFs) in response to tones of different pitch have sources that occupy different positions along the auditory cortex. The tonotopic organization of the human auditory cortex was first revealed in MEG experiments (Romani, Williamson, & Kaufman, 1982). The tonotopic organization of the human auditory cortex is described by Cosimo Del Gratta and Gian Luca Romani in chapter 10. Other imaging modalities have confirmed this finding. For example, single photon emission tomography has revealed a similar organization of the human auditory cortex (Ottaviani et al., 1997). Similar findings were obtained using functional magnetic resonance imaging (fMRI; Wessinger, Buonocore, Kussmaul, & Mangun, 1997).

Thus far, even after 20 years, this property of the auditory cortex has not been revealed in any AEP study, although an experiment with indwelling electrodes has confirmed the finding (Liegeois-Chauvel et al., 2001). So, even though the ultimate sources of the AEP and the AEF are the same, the two types of measures (MEG and EEG) differ in certain vital respects. We now make these differences clear.

Effect of Source Orientation

For the present it is useful to represent the sources of the MEG and EEG as equivalent current dipoles. Let us assume that the volume currents associated with an ECD underlie the EEG, and the field surrounding the ECD is a source of the MEG.

Many early MEG studies made the simplifying assumption that the head may be represented by a sphere the radius of which is approximately the same as the radius of curvature of the skull over which neuromagnetic measurements are made. As we shall see, this practice is beginning to give way to one in which more realistic head shapes are used (see chap. 3). For the sake of clarity, however, we stay with the older and still widely applied practice.

The sphere in Fig. 1.2A is 20 cm in diameter, and a current dipole is located 4 cm beneath its surface. It is very important to note that the current dipole is oriented at a right angle to a radius, that is, it is oriented tangentially with respect to the surface of the sphere. In practice, the field is measured simultaneously at many points about the sphere's surface. Each pickup coil of the *neuromagnetometer* used to detect the field is also oriented tangentially with respect to the surface. Therefore, it senses the radial component of the field, not its tangential component. Note that the radial component of the field is associated with the tangential

component of the dipole moment; the tangential component of the field is associated with the radial component of the dipole moment. It is customary to project these measurements onto a planar surface, which in this example has an area of 22.4 cm × 22.4 cm.

The radial component of the field is directed either outward or inward with respect to the surface of the sphere and does not include the component tangential to the surface. The strength of this radial component of the field varies with the place of measurement and is represented by the *isofield contours* shown in Fig. 1.2B. These isofield contours form a typical *dipolar field pattern.* It contains one region where the emerging field is at its maximum and another where the re-entering field is at its maximum. The centers of these regions are labeled *field extrema*. As one moves along a line defining the shortest path connecting these two extrema, a point is reached where the strength of the radial component of the field is zero. This zero point is precisely halfway between the field extrema. Moreover, the ECD lies directly under this point. Because our hypothetical measurements are restricted to the radial component of the field, the radial component has a value of zero halfway between the two extrema. As a matter of fact, the depth of an ECD lying directly beneath this halfway point is easily computed from the distance separating the field extrema on the surface of the scalp and the radius of the sphere that best fits the

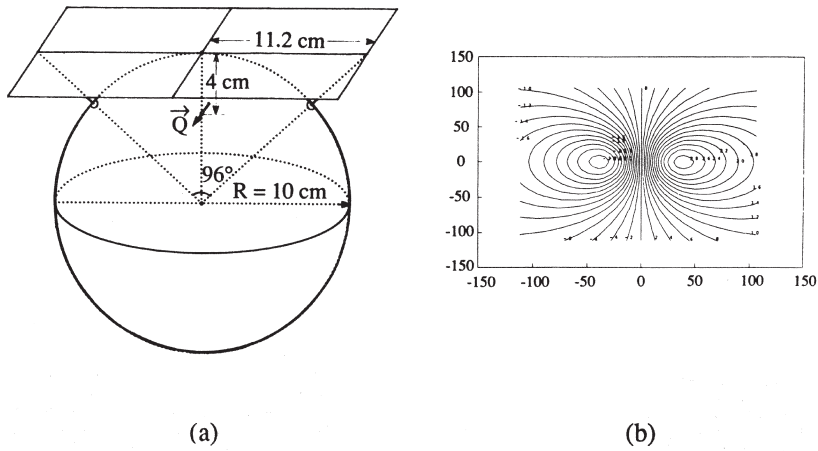

FIG. 1.2. Panel (a): schematic of a current dipole 4 cm beneath the surface of a 10-cm radius sphere. The radial component of the field is projected onto the surface of a rectangle tangential to the sphere. The center of the rectangle is directly over the point dipole. Panel (b): the isofield contour plot on the surface of the rectangle. The contours represent the relative radial field strengths in arbitrary units.

scalp on which those extrema are found. This insight made it possible to establish the tonotopic progression of sources along the auditory cortex (Romani et al., 1982).

Assuming that an ECD is 4 cm beneath the surface of a 10-cm radius sphere and oriented tangentially with respect to its surface (Fig. 1.2A), the relative strengths of the emerging and re-entering components of the field were computed. The isofield contours of Fig. 1.2B were then plotted. The computation is based on Equations 1.1 and 1.2.

$$\overrightarrow{B_{\vec{r}}} = \frac{\mu_0}{4_\pi} \frac{\vec{Q} \times (\vec{r} - \vec{r}_0)}{|\vec{r} - \vec{r}_0|^3} \qquad \textbf{(1.1)}$$

where $\overrightarrow{\mathbf{B}\vec{r}}$ = the field at a point $\vec{r}$ in space, $\vec{r}_0$ = the vector from the center of the sphere to the dipole, $\vec{\mathbf{Q}}$ = the current dipole moment, and μ_0 = the permeability of free space. Because the isofield contours of Fig. 1.2 represent only the strengths of the radial component of the field at the surface of the sphere, that component, $\vec{\mathbf{B}}$ ($\overrightarrow{\mathbf{B}_\mathbf{n}}$), is simply the dot product

$$\overrightarrow{B_n} = \vec{B} \cdot \vec{r} \,/\, |\vec{r}| \quad . \qquad \textbf{(1.2)}$$

If the dipole shown inside the sphere of Fig. 1.2 were tilted so that it is no longer tangential to the surface of the sphere, it could be described as being composed of two components, one oriented tangentially and the other radially. Ultimately, as the tilt increases, the dipole has no tangential component, because it is aligned with a radius extending from the center of the sphere to its surface. As the ECD is tilted from its initial tangential orientation, the dipolar field pattern at the surface simply diminishes in intensity. When the dipole's orientation is entirely radial, no radial field can be detected at the sphere's surface. It is interesting to note that the field pattern does not shift in position even as its intensity diminishes throughout the time that the dipole is rotating. The dipole would still lie directly beneath the point bisecting the distance between the field extrema. In other words, if the conductive volume is perfectly spherical, then measures at the surface of the sphere are sensitive only to the tangential component of the current dipole moment and not to the radial component of the current dipole moment.

The electric potential distribution across the spherical surface has different properties. As already indicated, the volume currents that accompany the current dipole produce potential differences across the surface

of the sphere. These may be represented by *isopotential* contours similar in appearance to the dipolar pattern of the isofield contours described earlier. (In attempts to achieve a more realistic model of the human head, three or four concentric spheres representing layers of different conductivity replace the single sphere shown in Fig. 1.2. These different layers result in a spreading or blurring of the isopotential contours, but it remains essentially dipolar when the underlying dipole is tangential to the scalp.) The most significant difference between the isofield and isopotential contours in this simple example is that the latter are rotated 90° on the projection plane with respect to the former. However, as the dipole is tilted from its tangential orientation, the positions of the isopotential contours shift and become asymmetrical. The potential at the extremum associated with the more distal (deeper) end of the underlying dipole grows weaker, while the extremum associated with the opposite pole (which is closer to the surface) grows stronger. The latter extremum migrates toward a point directly over the dipole, while the opposed extremum moves away from that point. Finally, when the dipole is oriented along a radius of the sphere, there is only one extremum on the surface. Of course, asymmetrical differences in conductivity within the head would result in greater differences between the patterns of isofield and isopotential contours.

The distinction between radial and tangential ECDs is important. For example, if the MEG represents tangential sources and the EEG represents both tangential and radial sources, it may be possible to subtract MEG data from some transform of EEG data and obtain an "image" of the radial sources. It is widely accepted that the radial sources dwell in the gyri of the cortex, while the tangential sources are to be found in the sulci. This could have obvious advantages.

Despite widespread recognition of this possibility, one must be circumspect with regard to its actual promise. For one thing, real sources of electric and magnetic fields in the brain are not point current dipoles; they are assemblies of many concurrently active neurons. Lu and Williamson (1991) estimated that the typical cortical area involved in coherent sensory-evoked responses is about 80–100 mm^2. A hypercolumn is composed of about 30,000 neurons, and several of these hypercolumns must be active if they are to produce a detectable field or a detectable difference in scalp potential. All neurons are bent, so any hypercolumn, even if it is largely normal to the surface of a gyrus, contains both radial and tangential components. Consequently, neurons in gyri will produce extracranial dipolar field patterns, although these are likely to be very

much weaker than if the same arrays of neurons were in the walls of a sulcus. Similarly, columns of neurons oriented approximately normal to the surface of a sulcus will have radial as well as tangential components. Hence, neurons in a sulcus may well contribute to the ostensibly "monopolar" isopotential patterns on the scalp associated with radially oriented sources. Hence, with sufficiently sensitive instruments, sources in gyruses would be detected in extracranial fields.

Although we emphasize that the skull is not a sphere, some truly remarkable results were achieved with the skull modeled as a best-fitting sphere (e.g., Romani et al., 1982). It is worthwhile to consider why this is the case.

The early assumption that the skull and scalp do not distort magnetic fields is now confirmed. The fields that emerge from and re-enter the skull are not altered by the presence of the skull and scalp (see chap. 2). Hence, one can effectively ignore the physical skull and scalp when measuring the radial component of the neuromagnetic field. Today, large arrays of detectors are usually arranged to fit the spherical surface of the tail section of the cryogenic dewars of neuromagnetometers. The fields penetrate this tail section without distortion. The surface of the tail section of the dewar is placed so that it is concentric with a sphere that best fits the head. The skull may not be perfectly concentric with the spherical array of sensors; hence, the measured field may include some contribution by the tangential field component. In effect, this introduces an error in the measured magnitude of the field. However, the position of a virtual current dipole placed at a known location in a model of a head can be determined with an accuracy of about 2 mm (Yamamoto, Williamson, Kaufman, Nicholson, & Llinas, 1988). Apparently, assuming that the head is spherical is not necessarily a major source of error in evaluating MEG data. This is not the case for the EEG, and one should consider this potential mismatch when attempting joint use of EEG and MEG data.

In a real head, a sphere with a particular radius of curvature may be a nearly perfect match to the curvature of the skull lying immediately above a current dipole source. The source may be radially oriented with respect to that particular sphere. However, the radii of curvature of adjacent regions of the skull may be different; hence, the same dipole is not exclusively radial in orientation with respect to those segments of the skull. It is obvious that a realistic head shape makes the distinction between radially and tangentially oriented dipoles somewhat ambiguous. Therefore, it is important to evaluate how realistic head shapes affect the measured electric and magnetic fields (see chap. 3).

MEASURING THE NEUROMAGNETIC FIELD

Ions flowing within neurons are surrounded by magnetic fields. Thus, intracellular ionic currents result in magnetic fields that surround neurons. Fields of different neurons do not interact with each other. Therefore, the measured field at a point in space is simply the sum of the fields contributed by each neuron. Because the field strength varies inversely with the square of the distance from a small (current dipole) source, a field measured at a point outside the human scalp would reflect the activity of relatively nearby neurons and be largely uncontaminated by fields of very distant neurons. As we shall see, suitably sensitive instruments make it possible to detect such fields of the brain. Thus far we have discussed fields associated with very simple sources, that is, ECDs immersed in a conducting solution enclosed by a nonconducting spherelike skull. Before turning to more realistic situations, we should introduce the methods used to measure the neuromagnetic field.

Fig. 1.3 is a schematic representation of a single-channel system that was used to measure the brain's neuromagnetc field. (It is important to note that existing systems use a very large number of sensors, and the single-channel shown here corresponds to only one of those sensors [see chaps. 7 and 8].) In Fig. 1.3, a magnetic field is shown emerging from one

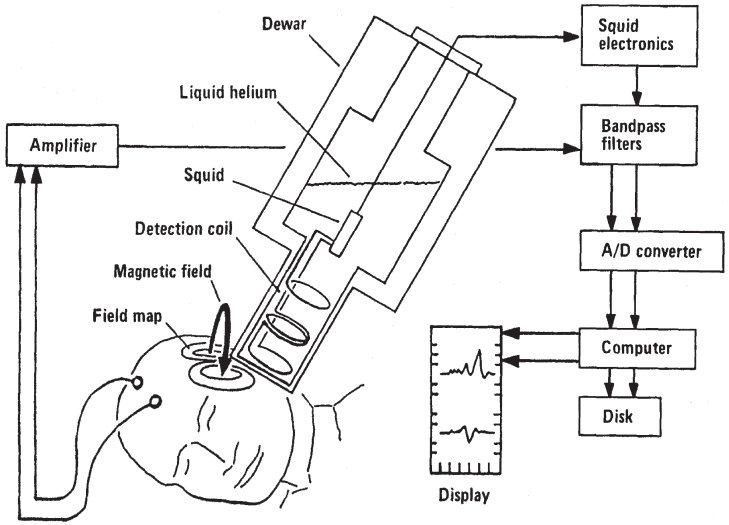

FIG. 1.3. Schematic of a single-channel neuromagnetometer measuring the brain's magnetic field. SQUID = superconducting quantum interference device.

region of of a subject's skull and re-entering a nearby region. The isofield contours represent those places where the emerging and re-entering fields have lesser values than the fields at the two extrema. The purpose is to measure the component of the field normal to the scalp at each of many positions.

The fields in question are extremely weak (about 50 femto Tesla), being on the order of 1 billionth the strength of the earth's steady field (= 50 micro Tesla), which is weaker than the fields of manmade magnets and motors as well as those associated with vibrating steel building frames and other urban sources of electromagnetic fields. This requires the use of an exquisitely sensitive instrument with a low intrinsic noise level and also capable of discriminating against extraneous magnetic fields. The sensitivity is provided by a device known as a *SQUID* (*s*uperconducting *qu*antum *i*nterference *d*evice), which operates at the temperature of liquid helium (4.2° K). Fig. 1.3 depicts a SQUID contained within a cryogenic *dewar* where it is immersed in liquid helium, along with other components. The field emerging from and re-entering the skull is undistorted as it passes through the bottom of the tail section of the dewar.

In Fig. 1.3 the field from the brain is sensed by the bottom-most (detection) coil of a set of coils within the tail section of the dewar. The complete set of coils (sometimes referred to as a *flux transporter*) is composed of a superconducting material such as niobium, which, at very low temperatures, has no resistance at all to the flow of an electric current. This particular configuration of coils is referred to as a *second-order gradiometer.* Roughly, this is how it works: Assume that we have a single loop of superconducting material in the dewar. If a magnet is nearby when liquid helium is poured over the coil (so that the loop enters the superconducting state), then the current will continue to flow around the loop for an indefinite period of time after the magnet is removed. The current flowing around the coil creates a magnetic field inside the superconducting loop. If the external field remains unchanged, the current remains constant and keeps the magnetic field inside the loop constant. In effect, the flowing current traps the enclosed magnetic flux (the *Meisner effect*). Thus, if the externally applied field should change, the current flow would change as well, to keep the trapped flux constant. The multiple coils in Fig. 1.3 are wound in series with each other and may be treated as though they are a single loop of superconducting material. So even here the flux trapped by the entire circuit remains constant.

Whenever a field is stronger near the bottom-most detection coil, the current flow will change in the entire gradiometer. In this example, the

detection coil is wound clockwise, while the next higher coil is wound counterclockwise. In fact, all adjacent coils in the loop are wound in opposition to each other. Thus, when placed in a uniform field the currents made to flow in these coils by the field would cancel each other out. Similarly, because the gradiometer is composed of four loops wound in opposition to each other (to form a *second-order gradiometer*), the application of a field with a uniform spatial gradient would also result in self-cancellation of any effect. Fields of distant sources tend to have uniform spatial gradients. However, a nonuniform field (one with high spatial derivatives, as shown in the figure) has a stronger effect on the bottom-most coil, and this leads to a net change in current flow within the entire gradiometer.

This property of second-order gradiometers makes them relatively insensitive to fields associated with distant sources. In effect, the operation of a gradiometer (as opposed to a simple *magnetometer,* which is composed of a single coil of superconducting material) is analogous to the common-mode rejection of noise that is made possible by bipolar electrodes in EEG recordings. A *third-order gradiometer,* which is composed of even more coils, is even less sensitive to uniform fields as well as fields with moderate spatial gradients. In fact, a well-balanced second- or third-order gradiometer makes it possible to measure weak neuromagnetic fields in many unshielded environments despite the presence of ambient magnetic fields (see chap. 7). However, to gain maximum sensitivity to signals of interest, for some purposes the dewar and the human subject or patient are usually placed within a magnetically shielded room.

The SQUID never "sees" the external field it is trying to measure. It is isolated within a superconducting shield inside the dewar, effectively isolating it from the environment. However, the gradiometer includes a very small *signal coil* wound in series with all of the other coils. Unlike the other coils, the signal coil is located inside the superconducting shield along with the SQUID. In fact, the only contact the SQUID has with the outside world is through the signal coil. Whenever a field is applied to the detection coil so that current flows throughout the gradiometer, the SQUID detects the current flowing in the signal coil, because that current is accompanied by its own magnetic field.

To describe this in more detail would distract us from our main objective. It suffices to say that the detection coils "sense" the magnetic field near the scalp, the signal coils "transmit" the currents in the detection coils to the SQUID, and the SQUID "converts" the currents in the signal coils to voltages that can be amplified and recorded by conventional elec-

tronic devices. The voltages are directly proportional to the magnetic field strength near the scalp. The single-channel system described here is based on the system designed and constructed by Brenner, Williamson, and Kaufman (1975) and used to detect the first evoked neuromagnetic field in an unshielded environment. However, as intimated earlier, this has been superseded by systems containing 200 or more SQUIDs. Also, the SQUIDs in use today are far more sensitive than the original SQUID and may be used with very different gradiometer configurations. For example, a gradiometer composed of several superconducting coils in a single plane may be used to sample differences in the radial field across the surface of the scalp. Such a configuration is described in some detail in chapter 9. Also, today sophisticated software is used to process signals from simple magnetometers to emulate different gradiometer configurations. Various whole-head systems are described in chapters 7–9.

Measuring the field at many places simultaneously permits identification of sources of neuromagnetic fields within the brain, thus overcoming one major problem. Early investigators had to assume that the source does not change from one measurement to another as a single-channel system is moved to sample the field at many different positions above the scalp. It is no longer necessary to make such an assumption.

EVENT-RELATED BRAIN ACTIVITY

It is obvious that the signals actually detected by neuromagnetometers are not produced by isolated current dipoles floating around in conducting solutions within spherical heads. However, in keeping with the didactic motive of this chapter, we approach more realistic situations slowly and in the process show why an elementaristic approach using spherical head models and point current dipoles has real value. We begin by considering Fig. 1.4.

It has been known for many years that activity in the brain stem may be evoked by acoustic stimuli and picked up by scalp electrodes. The extremely weak auditory brain stem evoked responses begin to appear about 2 msec after the onset of stimulation and run their courses before much stronger responses of the auditory cortex are picked up. On occasion, the latter are seen after a single stimulus event and are certainly strong enough to be detected reliably after averaging a few dozen trials. However, the brain stem activity must be averaged over several thousand trials to be detected. With the exception of this type of brain stem activity, most brain activity seen in the EEG or the MEG originates in the den-

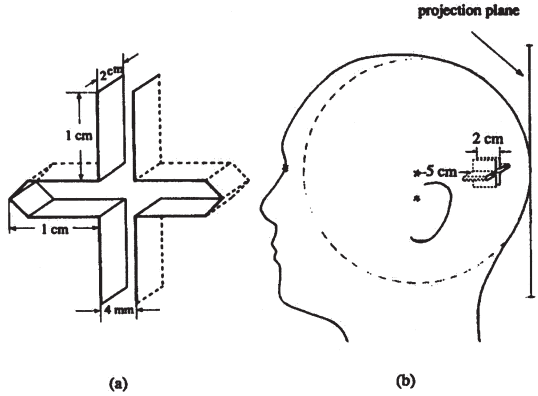

FIG. 1.4. Cruciform model of the visual cortex.

drites of cells of the cerebral cortex—in the gray matter of the brain (see chap. 12 for examples of signals that may well be attributable to fields associated with spike potentials). As we shall see, this is enormously helpful in determining the approximate location in the brain of the sources of observed evoked magnetic fields.

The cortex of each hemisphere may be thought of as a two-dimensional but highly rumpled (convoluted) sheet of neural tissue. Although it is about 2 mm thick, this thickness is negligible when fields are measured at a distance. It is useful to think of this two-dimensional sheet as populated by a very large number of dipolar sources, all oriented normal to its surface. (We conducted computer simulations in which the individual dipoles of a large array are randomly tilted by as much as 45° from the normal. The summed isofield contours describing the radial component of magnetic fields at the surface of a spherical skull are essentially the same as when all of the dipoles are normal to the surface.) Of course, the dipoles represent aggregates of cells.

The cerebral cortex contains approximately 10 billion cells. Even if the cells were independent of each other, on occasion, by chance alone, ionic currents within significant numbers of them would flow in the same direction at the same time. We refer to this as *synchronization.* In many instances this synchronization is initiated by some external or internal event. Where the initiating external event is a sensory stimulus—for example, a flash of light—we refer to a *sensory-evoked response.* Where the sensory stimulus results in the flow of current within a sufficient number of neighboring columns of cells within the same window of time (the activity need not start or end at precisely the same time), then it may be possible to pick up either an evoked potential or an evoked field. It has been estimated that something on

the order of 100,000 concurrently active cells may be sufficient to produce a detectable extracranial neuromagnetic field. The visual cortex is a useful example. The central 2° of the retina (the *fovea*) is known to affect roughly 25% of the entire primary visual cortex (Brodmann's area 17). It is worth noting that the diameter of the entire fovea corresponds to a ~0.5-mm diameter image of a disk on the retina. This small patch of light centered on the retina could affect much of the occipital pole as well as a large area extending deeply into the longitudinal fissure, including the calcarine fissure. If the same small patch of light were moved away from the fovea and into the peripheral visual field, it would affect a very rapidly decreasing proportion of the cortex extending into the longitudinal fissure. The shape of the visual cortex is schematized in Fig. 1.4. This crosslike shape is sometimes referred to as the *cruciform model* of visual cortex. The calcarine fissure represents the arms of the cross, and the longitudinal fissure is the space between the two halves of the cross. Real brains lack this degree of symmetry, but the model is useful in several respects. First, it helps in explaining the retinotopic organization of the visual cortex and, second, it clearly illustrates how the shape of the brain might affect its observed neuromagnetic field.

Figure 1.5 illustrates how different regions of the visual cortex are excited when appropriate stimuli are placed in different quadrants of the visual field. The neurons of the cerebral cortex are arranged in columns oriented normally to its surface, so activation of the lower left quadrant of the cruciform model must result in a net flow of current either inward (away from the surface) or outward. Thus, it is possible to activate a rather large area of the cortex merely by presenting a moving or flashing pattern in an appropriate retinal location. The vast majority of columns of cells in these activated areas may be conducting current in the same direction at more or less the same time. Intuitively, this source of evoked activity is a far cry from a point current dipole.

The unshaded areas of cortex are also active. The cells in the unshaded areas are synchronized with each other by chance alone. For our purposes we may assume that the columns of cells filling the unshaded regions are randomly active; that is, the direction and magnitude of net current flow in one column cannot be predicted from that of its near neighbors. In point of fact, at any instant of time this random activity effectively masks the more coherent activity of the columns within the shaded areas. This explains why *signal averaging,* or some other method for enhancing signals relative to "noise," is needed to recover evoked fields and potentials.

Kaufman, Kaufman, and Wang (1991) computed the isofield patterns associated with synchronized activation within the shaded areas shown

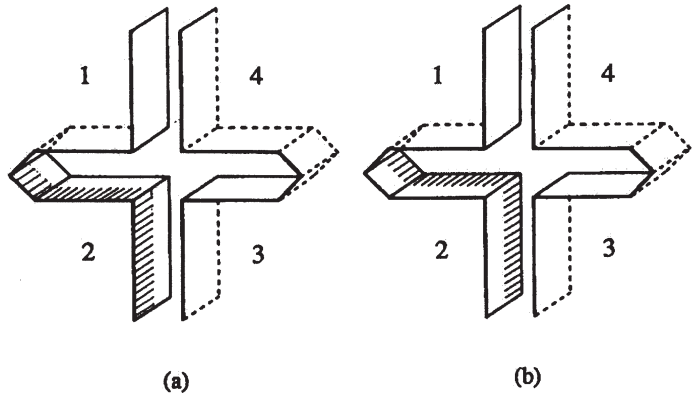

FIG. 1.5. A simulation in which the upper right quadrant of the visual field activates cortical cells of the lower left quadrant of the cruciform visual cortex. The shaded region in Panel (a) lies closer to the occipital pole and illustrates a possible distribution of activity evoked by stimulation in the upper right quadrant of the fovea. As the stimulus is moved away from the fovea and farther into the peripheral field, the depth of activity along the cortex shifts inward, as indicated by the greater depth of activity signified by the shaded area of Panel (b). The dipoles (columns of cells) in the shaded areas are oriented normal to the surface of the cortex.

in Fig. 1.5. Specifically, they assumed that the shaded areas covered many dipoles, all oriented normal to the shaded surface. The only difference between Fig. 1.5A and Fig. 1.5B is that the shaded area in the latter is 1 cm deeper than the similar shaded area of Fig. 1.5A. The magnitudes of these dipoles were randomized, but their directions were the same, signifying that they are all synchronized with each other. In this simulation the large unshaded areas of the entire cruciform cortex were populated by unsynchronized dipoles, that is, dipoles whose moments were all randomized. On average, the magnitude of current flowing in the synchronized dipoles was the same as that in the unsynchronized dipoles, although different values were selected at random every time the field at the surface of the skull was sampled. Overall, in this simulation the cruciform cortex was populated with 1,386 current dipoles. By superposition, the radial component of the field at the surface of the spherical head due to all of the dipoles was computed at 841 points, and these were plotted to form the isofield contour plots projected onto a plane. Several such plots are shown in Fig. 1.6. One hundred plots were computed to illustrate how the pattern of isofield contours changes because of random contributions by the asynchronous dipoles.

The asymmetries of the two lefthand isofield contour plots in Fig. 1.6A and Fig. 1.6B are due to random contributions by the dipoles that populate

the unshaded walls of the cruciform cortex. These asymmetries cannot be accounted for by assuming that a single current dipole underlies the observed field. Instead, a much better fit is achieved when one assumes that multiple dipoles contribute to the field. However, this pattern changes from one set of measurements to another. Averaging sharply reduces this variability, because the randomly varying moments of the dipoles that populate the unshaded regions tend to be self-canceling when their fields are averaged, and the resulting plot is a much closer fit to the pattern that would be produced by a single equivalent current dipole. Hence, a field pattern produced by hundreds or even thousands of dipoles can easily be confused with a pattern produced by a single equivalent current dipole.

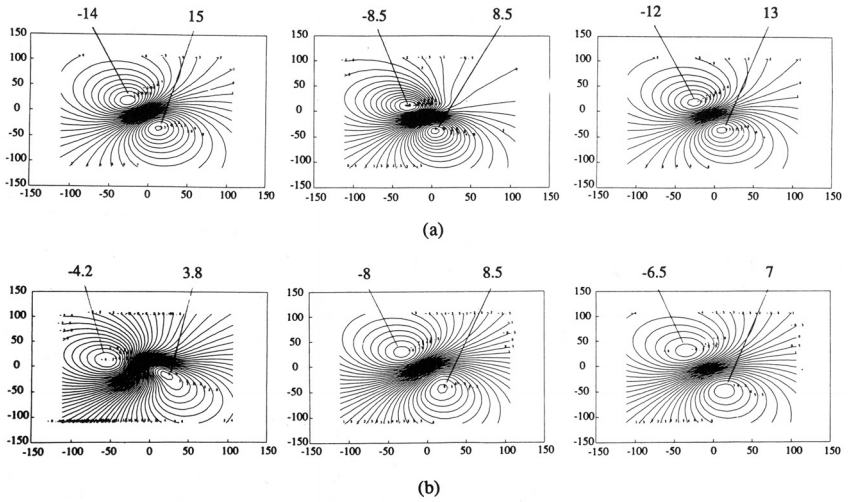

FIG. 1.6. Isofield contour plots associated with activation of a large number of current dipoles oriented normal to the surface of the cruciform cortex. The three plots in the upper row (Panel [a]) of the figure are based on synchronized activity in the outermost shaded area illustrated in Fig. 1.5. The two plots on the left side of (a) were selected at random from 100 such plots, where each corresponds to a different set of dipole moments. These 100 plots were averaged to produce the third plot on the right of (a). Note that the average values of the field extrema in this plot differ in magnitude from the two to its left. Also, the plots on the left are not as symmetrical as the average plot. The latter is best fit by the field that would be produced by a single equivalent current dipole. The relatively asymmetrical patterns on the left reflect contributions of dipoles dwelling in the unshaded portions of the cortex. Some subset of these dipoles would be synchronized with the evoking stimulus by chance alone. The three lower plots (Panel [b]) are based on synchronization of the (1-cm) deeper shaded area of Fig. 1.5B. Here, too, the single "trial" plots to the left are asymmetrical and differ in orientation and magnitude from each other and from the average plot on the right. Note that the space separating the average field extrema in (b) is wider than that of the righthand plot of (a).

Comments on Signal Averaging

Readers who are familiar with signal averaging may choose to skip this section, but several of its passages may prove to be worth scanning. Some subtle and frequently overlooked assumptions underlie this simple procedure for recovering signals from noise, and it is good to keep them in mind. For example, if the so-called "signal" (the event-related response) is not independent of ongoing asynchronous activity of the brain, then averaging can lead one to discard important data along with the noise. This is quite relevant to our discussion of spontaneous brain activity.

Figure 1.6 provides a demonstration of the effects of signal averaging. Isofield contour plots similar to those shown in Fig. 1.6 can be thought of as instantaneous maps of the field obtained by many sensors at once. One hundred such maps were generated as follows: One hundred independent sets of random numbers were generated to represent the current dipole moments (directions of current flow and their magnitudes) of all the dipoles in the unshaded areas of Fig. 1.5. This is the region that is assumed to be unaffected by the presentation of a stimulus. Similarly, the dipoles under the shaded areas were also represented by 100 independent sets of random numbers, but these represent only their magnitudes, as the direction of current flow was the same for all of the dipoles. The commonality of direction of current flow in this region is assumed to be due to the action of a stimulus or event that has the effect of synchronizing the neurons within the shaded regions. All of these values were used to compute the fields represented by 100 different isofield contour maps, represented by the samples in Fig. 1.6. The 100 contour maps derived from the more shallow shaded area were then averaged to create the plot on the upper right side of the figure. Similarly, another 100 maps were averaged to create the lower plot on the same side of the figure. This averaging process reveals a contour plot largely due to the synchronized activity of the neurons under the shaded patch of the cortex. The cortex is normally active, regardless of whether a stimulus is present. Therefore, a sensor placed above the occipital cortex will detect a magnetic field at all times. Because of the asynchronous activity of the neurons that contribute to this field, its direction and strength will be different from time to time. However, when the field is repeatedly measured at a fixed time after the presentation of a stimulus, the field due to asynchronous activity will tend to be self-canceling, whereas averaging will reveal the synchronized activity evoked by the stimulus. Activity time-locked to the stimulus will increase arithmetically with the number of samples taken, whereas the presumably Gaussian background noise (due to the asynchronous activity,

instrumentation noise, and ambient noise) will increase only as the square root of the number of samples. Although in realistic situations the background noise on a single trial is much greater in magnitude than the evoked response, when a sufficient number of samples enter the average, the evoked response ultimately becomes significantly larger in amplitude than the noise. All of this assumes that the noise is independent of the evoked response. Much of the literature tacitly assumes that a change in voltage or field that is time locked to the evoking event is the only relevant consequence of stimulation. As we shall see, this assumption is often invalid.

Are Event-Related Voltages and Fields Independent of Brain Noise?

The logic underlying this section is quite simple. We begin by assuming that neural tissue is active regardless of whether a particular external stimulus is presented. The activity may be due to intrinsic biochemical changes, activity originating in the thalamus and transmitted to the cortex, or any of several possible conditions. The external stimulus, on reaching the cortex, may well interrupt or alter this ongoing activity. Hence, if the stimulus causes the current flow within a neuronal population to be synchronized, it may also either add to (or subtract from) the ongoing activity. If the evoked activity merely adds linearly to the ongoing activity, then, in effect, it is independent of that activity, and the time-locked response is the only consequence of stimulation. However, if the level of activity of the affected neurons is not the linear sum of the ongoing activity and of the evoked activity, then consequences of stimulation may not be detectible in the averaged response.

Linear and Nonlinear Systems. Any system, whether it is an electronic circuit or a portion of the nervous system, can be described as being either a *linear system* or as a *nonlinear system.* If two signals are applied concurrently to a linear system, the output of that system is equal to the sum of the outputs of the same system to the same inputs presented at different times. In this case, we say that the *superposition principle* applies to the system. When the superposition principle does not apply, we say that the system is nonlinear.

If a sinusoidally varying signal is applied to a linear system, then its output will be a sinusoid at the same frequency as the input. Although the amplitude of the output may not be uniform for inputs of different frequency, a linear system always responds at the same frequency as that of the input. It has been known for some time that visual responses

evoked by sinusoidally modulated light often occur at twice the frequency of the stimulus. Any system that responds to an input of one frequency with an output of another frequency is necessarily nonlinear.

Figure 1.7 explains how frequency doubling occurs in the case of one nonlinear system. In this case, the output of the system is the square of the input. (The same is true if the output is proportional to the square of the input, except that the proportionality constant defines the amplification afforded by the system.) Thus, where the input is $a \sin \omega t$, the output

$$\mathbf{Y_{output} = (}a^2 \sin^2 \omega t\mathbf{)} \quad . \tag{1.3}$$

From elementary trigonometry,

$$A^2 \sin^2 \omega t = a/2 - a/2 \cos 2\omega t \quad . \tag{1.4}$$

As in Fig. 1.7, this demonstrates that, when squared by a nonlinear system, a sinusoidal input (frequency = ωt) with amplitude a results in an output at twice the frequency of the input ($2\omega t$) and one half the am-

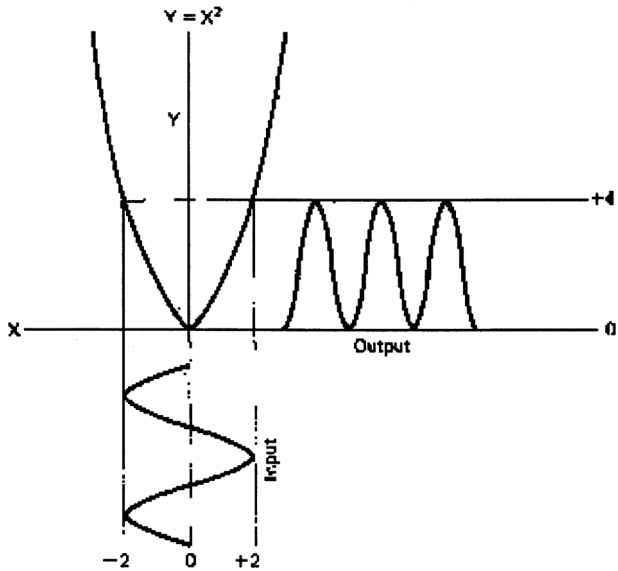

FIG. 1.7. Effect of applying a sine wave (input) to a device whose output is the square of the input. The graph represents the equation $Y = X^2$. Note that the sinusoidal input has a mean value of zero and, in arbitrary units, its amplitude peaks at 2 and –2. The output amplitude peaks at 4 and 0, so it happens to be the same (4 units) as that of the input. However, the average of the squared output is one half the peak-to-peak amplitude, and the output contains a sine wave.

plitude of that frequency. Furthermore, the output has a Fourier component which, in this case, has an amplitude $a/2$ and a frequency of zero (a *dc* component).

Squaring is not the only form of nonlinearity. For example, many biological systems transform an input stimulus so that the response of the system is approximately proportional to the logarithm of the stimulus.

The output of such a system to a sinusoidal signal oscillating about an average value of zero (as in Fig. 1.8) contains a *dc* offset and odd harmonics of the frequency of the input. Similarly, systems that clip the smoothly varying positive and negative peaks of sine wave inputs also generate odd harmonics.

Half-wave rectifiers are sometimes referred to as *linear rectifiers*. These are not linear at all; rather, their outputs represent only the positive (or negative) peaks of sinusoidal inputs, and these too contain odd harmonics of the input. In general, the relative amplitudes of these harmonics depend on the nature of the nonlinearity and on whether the input signal is a simple sine wave or if it can be represented as the modulation of a steady *dc* signal. In fact, if the *dc* component of the input is large relative to its sinusoidal modulation, the effect of the existing nonlinearity may become negligible. Incidentally, this is one of the main reasons why researchers studying the response of the visual system to sinusoidally modulated light may use a near-threshold degree of modulation of a steady light as a stimulus. Despite its inherent nonlinearity, when presented with such a stimulus the visual system is approximately linear in its behavior. It is sad that real eyes evolved to deal with large-scale changes in visual stimulation, so allowing for effects of nearly pervasive nonlinearity is essential to understanding the perceptual process.

Nonlinearities exemplified by different kinds of rectification—for example, square law—have quite different effects from those attributable to saturation, for example, when a sensory stimulus is so intense that an otherwise linear system ceases to respond to additional increases in its intensity. We do not consider such effects here except to say that in some evoked-response experiments investigators fail to use a range of stimulus intensities—for example, contrast or loudness—that include very low values as well as high ones. This is the only way to determine if the observed responses are influenced by saturation nonlinearities rather than some other ostensible cause.

Interactions of Signals at Different Frequencies. Thus far we have not dealt directly with the interaction between the response of the brain and its ongoing activity. It is easier to understand how such an in-

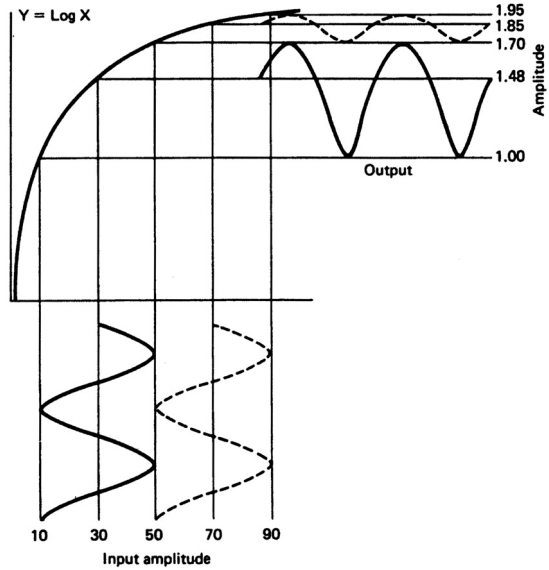

FIG. 1.8. The output of this nonlinear system is proportional to the logarithm of its input. As demonstrated here, a sinusoidal input is distorted by the system so that its output is not a pure sine wave. In this case the distortion is most obvious when the input is low (solid line) and less obvious when the input rides on a high *dc* (dashed line). This is one reason why vision researchers superimpose a sinusoidal variation in light level on a *dc* "pedestal."

teraction may come about by describing what happens when two signals of different frequencies are applied concurrently to the same nonlinear system. As stated earlier, in a linear system the response to concurrent stimuli is the same as sum of the responses to the two stimuli applied separately. It is extremely important to note that even if the brain as a whole were essentially nonlinear, if the two stimuli were to affect different regions so that no interaction is possible, then the response would also be the same as the sum of the responses to the two stimuli when applied separately. In chapter 5, Regan and Regan exploit this distinction to gain insight into how signals are parsed by the sensory systems. For now we deal only with the case where two different signals are applied concurrently to the same nonlinear system.

Suppose that lights are modulated at two different frequencies, and the frequency of one is not a harmonic of the other. For example, one light is modulated at 7 Hz and the other at 10 Hz. Both lights are imaged in the same place on the retina. When a signal-averaging computer is time locked to a signal at 7 Hz, then a response is usually recovered at that frequency or,

on occasion, at its second harmonic, that is, 14 Hz. Similarly, when time locked to the concurrently presented 10-Hz stimulus, a response is recovered at 10 Hz and at its second harmonic, that is, 20 Hz. It is interesting to note that when the 7-Hz and 10-Hz signals that drive the two stimuli are multiplied, the output of the multiplier does not contain signals at either 10 Hz or 7 Hz. Rather, the output is at 3 Hz (the difference between 7 and 10 Hz—the so-called *difference frequency*) and at 17 Hz (the *sum frequency*). If the output of the multiplier were applied to a signal-averaging computer time locked to either of the original 7- and 10-Hz inputs to the multiplier, the averaging computer would reveal no signals whatsoever. This is because the sum and difference frequencies are not integer multiples of 7 or 10 Hz. Now suppose that when the two stimuli are presented to a subject, some of the affected portions of the nervous system are nonlinear. The result is that the nonlinearities produce sum and difference frequencies, and these cannot be recovered when a signal averager is time locked to either stimulus. It is of some interest to note that Helmholtz (1885/1954) postulated the presence of nonlinearities in the auditory system to account for the so-called *combination tones*. These are perceived when a listener is presented with two different pure tones far enough apart in frequency so that one does not hear ordinary beats. In chapter 5, Regan and Regan describe several kinds of nonlinearity and how it results in the generation of frequencies that are not harmonics of concurrently applied stimuli. Taken together, the bands of frequencies generated by nonlinear interactions are referred to as *sidebands.* Using a very sensitive spectrum analyzer rather than an averaging computer, Regan and Regan were able to discern the presence of sidebands when the subject is stimulated and their absence without stimulation. These sidebands do not contain components that are harmonics of the applied stimuli. As Regan and Regan point out, this information may be invisible to the averaging computer, but it can still be retrieved and used to gain insights into the nature of neural processes underlying sensory phenomena. For example, detecting frequency components that are a consequence of stimulation but are unrelated harmonically to the stimuli is a powerful way to determine where in the brain inputs from different sense modalities produce effects that interact with each other.

We now illustrate this point with a hypothetical experiment. Suppose that a periodic visual stimulus is presented to the eyes and that periodic acoustic stimuli are presented to the ears. If the two types of stimuli are not harmonics of each other, then an averaging computer can easily detect the separate and independent responses they evoke in the visual and auditory parts of the brain. Regan and Regan (1987) used this approach to de-

termine whether independent channels exist within single-sense modalities, for example. In our hypothetical experiment one can set the sweep duration of the averaging computer so that it corresponds to the period of the visual stimulus and then to the period of the acoustic stimulus. The visual and auditory responses would emerge from the background noise. If the neural effects of these stimuli should interact with each other, then a high- resolution spectrum analysis can reveal the presence of the products of the interaction, that is, sidebands. By mapping the fields about the scalp that fluctuate in step with frequency components of the sidebands, it is possible to locate the regions of the brain in which the interactions occur, as these regions may be represented as current dipoles. This appears to be a very promising line of research that should be pursued by researchers working in EEG as well as in magnetic source imaging (MSI).

In this chapter, however, our concern is less with the sidebands generated by concurrently presented stimuli than with the question of the independence (superimposability) of effects of sensory stimuli and the ongoing activity of the brain. However, the same basic principles apply.

Models of cortical circuits may incorporate extracortical oscillators that lead to apparently spontaneous changes in neuronal membrane potentials. So, for example, signals originating in the brain stem activate cortical neurons at the frequencies of the alpha rhythms. Similarly, when a sensory stimulus is applied to the organism, signals travel along thalamocortical pathways to evoke cortical activity. These evoked responses may well interact in the cortical neurons with the effects of signals from the hypothetical extracortical oscillators. In this case the evoked response would modulate the so-called "spontaneous activity" of the affected cortical neurons (Kaufman & Locker, 1970).

Cross-Modulation of Evoked Response and Spontaneous Brain Activity. When a response evoked at one frequency interacts with a concurrent response evoked at some other frequency, one says that each response modulates the other. In fact, this is precisely what happens when an electric signal at acoustic frequencies is used to modulate another electric signal at a radio frequency to produce an amplitude-modulated wave for radio transmission. The modulated wave is composed of the original radio frequency signal plus sidebands composed of the sums and differences of the original acoustic signal and the radio frequency signal. By contrast, ongoing brain activity is not a spectrum of discrete frequency components; rather, the spectrum is continuous. As a result, the sidebands are not composed of discrete spectral lines. They, too, form a

continuous spectrum. Despite this difference, we shall see that the ongoing activity of the brain can be altered or modulated in amplitude when a response is evoked by a sensory stimulus.

The presence of this modulation is proof of two things: first, that the brain responds in a nonlinear manner to incoming signals, and second, that the measured activity of the brain is not independent of the so-called noise represented by the brain's spontaneous activity.

Hans Berger, the discoverer of the EEG, also discovered a phenomenon he described as *alpha blockage.* A frequency band ranging from about 8 Hz to 12 Hz predominates in the EEG measured over the occipital region of the brain. This is the so-called *alpha band.* It is strongest when the subject is resting with eyes closed and diminishes dramatically if subjects open their eyes and become alert and attentive. During this state of alpha blockage the EEG is dominated by activity in a band around 20 Hz or, roughly, twice the alpha frequency. This so-called *beta* activity is weaker in amplitude than the alpha activity it purportedly replaces. It should be noted that activity at roughly 8 Hz to 12 Hz tends to be predominant over most of the scalp, but when it appears to arise in the region of motor cortex it is referred to as *mu* activity. For the purposes of this chapter we refer to all activity in this frequency band as alpha. In any event, an early and still widely accepted theory is that activity in the alpha band is due to the synchronization of many cortical neurons whose electric fields tend to oscillate at a frequency in a band surrounding 10 Hz. According to this theory, the replacement of alpha by beta is due to the desynchronization of the neurons, which occurs when the neurons are activated. The ostensible desynchronization implies that the individual neurons still oscillate at alpha frequencies, but the fields of these neurons tend to be self-canceling when they are out of step with each other. So, according to this view, the lesser energy detectable at beta frequencies really means that the neurons are more active, rather than less active, during alpha blockage. On the basis of this, one can claim that alpha blockage is not due to a suppression of alpha activity that goes on independently of any other activity in which the neurons might become engaged. However, when otherwise engaged, the neurons are no longer idling along in a synchronous fashion. Hence, by this theory, the signal (which results in activation) is independent of the noise. However, evidence suggests that this view may not apply.

It seems likely that event-related or -evoked activity modulates ongoing activity of the brain, which implies that the evoked response is not independent of the so-called noise. We should also note that computer simulations of a sheet of asynchronous dipoles oriented normally to the surface of

the walls of a sulcus show that more field power may be produced when the dipoles are synchronized than when they are desynchronized (Kaufman et al., 1991). This depends on the geometry of the cortex, especially its symmetry. In the EEG domain, synchronized dipoles located in the gyrus may actually produce higher voltages at the scalp than when they are asynchronous. In any event, it is far from proven that alpha blockage is due solely to desynchronization; it may also be due to some kind interaction of event-related activity and spontaneous activity.

Measuring the Interaction. One way to determine whether evoked activity interacts with spontaneous activity is to examine the entire frequency spectrum of the brain's magnetic or electric fields. This could reveal that energy is added at frequencies that are not harmonics of the fundamental frequency of the stimulus. During signal averaging such frequency components would be discarded along with noise. Thus far, little research has used this straightforward approach. However, an indirect method has revealed the presence of modulation of brain activity by event-related activity.

Kaufman and Price (1967) developed this indirect method to examine high-frequency cortical activity (300 Hz–1000 Hz) associated with visual stimulation. This is the same band of activity that Hashimoto discusses in chapter 12. Kaufman and Price recognized that a 1-msec pulse (as in the action potential) has a frequency spectrum containing energy at frequencies ranging from *dc* to about 1 kHz. As it happens, the frequency spectrum of a single impulse is essentially the same as that of an infinite number of randomly occurring identical impulses. Therefore, if a large number of impulses occur in a more or less random sequence across many neurons within the same interval of time, it is theoretically possible to detect activity at frequencies well above the range of the normal EEG (*dc* – ~60 Hz) with scalp electrodes. The stimulus was a light flashing at 15 Hz. The output of a wide-band amplifier measured the voltage across two scalp electrodes over the occipital cortex. The output of the amplifier filtered to pass activity between 300 Hz and 1000 Hz. This activity was then squared (rectified) and applied to a low-pass filter. A lock-in amplifier was used to detect activity in the rectified EEG at 15 Hz that was time locked to the stimulus. The presence of such activity would indicate that the high-frequency band was modulated by evoked activity at the frequency of the stimulus. A statistically significant response was found. This indicated that visual stimulation resulted not only in an evoked response at the frequency of the stimulus but also in side bands that were

not harmonics of the stimulus. These side bands happened to be in the high-frequency domain. Essentially this same method has revealed that activity in the low-frequency band of the normal EEG and MEG is also modulated by sensory stimulation and other events.

Assuming that a 15-Hz visual stimulus does not evoke responses containing harmonics above 150 Hz, the responses detected after squaring the 300 Hz–1 KHz band can be thought of as the variance about a mean zero response. (Actually, assuming them to be present, Kaufman and Price [1967] undertook to remove such high harmonics, and the remaining noise was still modulated at 15 Hz.) Kaufman and Locker (1970) used this same procedure to demonstrate a similar modulation of harmonically unrelated activity within the normal EEG band by a visual stimulus.

The variance about a mean response of zero is proportional to *power*. Voltage is often expressed in terms of *rms* (root mean square) volts. It should be noted that *rms* voltage is mathematically identical to the familiar *standard deviation* of statistics, which, in turn, is the square root of variance. Hence, *electric power* is the same as variance (voltage squared), whereas *field power* is equivalent to field squared. Several studies have revealed that MEG and EEG power fluctuate during the performance of several different cognitive tasks, for example, memory search for tones and for visual forms, as well as during a mental rotation task (Kaufman, Curtis, Wang, & Williamson, 1991; Kaufman, Schwartz, Salustri, & Williamson, 1990; Michel, Kaufman, & Williamson, 1993; Rojas, Teale, Sheeder, & Reite, 2000). In these studies it was found that the duration of a profoundly reduced level of alpha power was highly correlated with time to scan memory for tones or forms as well as to signal completion of a mental rotation task. The distribution of affected field power across the scalp appeared to differ with the modality involved, and was therefore not a generalized effect of, for example, heightened alertness. The affected activity is not synchronized with any stimulus event, although the modulation of its power is related to the time required to perform the task. ERP and event-related field (ERF) studies of short-term memory search and many other cognitive tasks reveal differences in amplitude of various response components, but in most studies these are not as well correlated with the time required to complete the task.

It is clear that background activity is affected by stimulation and by performance of cognitive tasks. These effects are not mirrored in the standard ERP or ERF. Hence, this is an area that should be explored more extensively. For the present it suffices to stress the following point: The so-called noise rejected during signal averaging may well contain signifi-

cant information related to sensory responses and cognitive processes. This could involve specific regions of the cortex, depending on the modality and the nature of the task. One way to begin to study the relation between this information and mental processes is simply to compute the variance within different frequency bands about the average response. This is well within the capabilities of modern desktop computers, so researchers no longer need to rely solely on differences between average responses both within and across subjects, which is the traditional way to study response reliability and its inverse, variability.

LOCATING THE SOURCE

One of the ostensible advantages of MEG is that the radial neuromagnetic field is not distorted by the intervening bone, skin, and other tissues. Hence, in principle it should be simpler to locate the source of the observed field than it is to do so on the basis of EEG measures. Because evidence suggests that spontaneous activity originating in specific regions of the cortex may be differentially affected by cognitive tasks, it is of some interest to inquire as to how well one might locate those regions on the basis of field or field power data. Wang and Kaufman deal with this particular issue in some detail in chapter 4. We shall briefly introduce the same topic here, beginning with the much simpler problem of locating the source of a neuromagnetic field when that source is modeled as an equivalent current dipole.

The Problem With the Inverse Problem

Brenner, Lipton, Kaufman, and Williamson (1978) stimulated the little finger of one hand with a periodic electric impulse. This evoked a neuromagnetic field in a confined region over the hemisphere contralateral to the stimulated finger. The investigators measured the radial field at many places across the scalp. The same stimulus was applied to the thumb of the same hand, and the field pattern was measured again. As expected, the field pattern associated with the stimulation of the little finger contained a region where the field was directed outward from the head and, at the same time after stimulation, another region where the field was directed inward. The same polarity reversal of the field pattern was associated with the stimulation of the thumb, but one important difference was evident in the empirical isofield contour plots: The field extrema associated with stimulation of the little finger were about 2 cm lower on the scalp than those associated with stimulation of the thumb.

Furthermore, these field extrema were located approximately above the projection of the central sulcus onto the scalp. The source of activity evoked by stimulation of the little finger is located along the posterior bank of the central sulcus and about 2 cm lower down than the source of activity evoked by stimulation of the thumb. This was probably the first empirical evidence that it is possible to identify the locations of current dipole sources on the human cerebral cortex, and it led directly to many studies in which ECD localization was based on neuromagnetic field measurements. As Wang and Kaufman discuss in chapter 4, it is possible to compute the field everywhere outside a sphere filled with a conducting fluid and containing a current dipole of a given strength, orientation, and position. One, and only one, field pattern can be attributed to this dipole. Hence, one says that there is a unique solution to the so-called *forward problem.* However, is not possible to determine the strength, orientation, and position of a current dipole solely on the basis of the observed external field. This follows from the fact that any number of dipoles or combinations of dipoles could produce the same field. When one considers that all actual measurements are accompanied by noise, the uncertainty surrounding the validity of any putative source of the observed field is even greater. Even without this uncertainty, in principle it is impossible to discover a unique solution to the so-called *inverse problem.*

Investigators attempting to identify sources of observed field patterns (such as those associated with the little finger and thumb) resort to different strategies. We do not consider all of them here, but most begin with an informed guess as to the location of the source, for example, normal to the posterior bank of the central sulcus when studying responses to stimulation of a finger. Computer simulations may be used in which a current dipole is placed at a particular location in a sphere that best fits the subject's head, isofield contours plotted on the basis of solutions to the forward problem using Equations 1.1 and 1.2. The fit of these contours to those that were actually observed is tested. The moment, depth, and orientation of the dipole is then altered in an iterative fashion until a best fit (in the least squares sense) is achieved. The computed position of the dipole is then plotted in a magnetic resonance imaging scan. A similar procedure may be used when dealing with pathological states in which particular waveforms recur with some frequency (e.g., interictal spikes in the MEGs of some epileptics). When the computed positions of ostensible dipole sources are plotted in magnetic resonance imaging scans of such patients, the ECDs are often found to be in or near observable lesions. In some cases the lesions cannot be visual-

ized, but surgical procedures have revealed small tumors near the computed sites of the ECDs.

A single equivalent current dipole may well account for an observed field pattern, and, when noise is relatively low, one might achieve an even better fit by assuming contributions of quadrupolar and possibly higher order sources. This alone is a useful but relatively modest accomplishment when compared with a larger goal of MSI. As we have taken pains to point out, the actual sources of observed fields are extended distributions of currents on the cerebral cortex. Many investigators have been tantalized by the possibility of finding a way to describe these extended distributions of current based on measurements of the brain's magnetic field. In chapter 4, Wang and Kaufman cite and briefly describe some of these efforts. They describe one such approach, the *minimum norm least squares* (MNLS) inverse, in some detail, along with results of computer simulations. The simulations were designed to demonstrate that there are circumstances in which it is entirely feasible to find a unique solution to the problem of describing the spatial distribution of currents on the cortex. Solutions to these inverse problems primarily require accurate knowledge of the geometry of the surface of the cortex and also assume that the elements of current that make up the distribution flow normal to the surface of the cortex. In principle, given a properly constrained problem, it is possible to arrive at a unique solution to the inverse problem of describing distributed current sources of observed magnetic fields. The MNLS inverse described by Wang and Kaufman has not yet been tested using real MEG data. Sufficiently large arrays of sensors were not available at the time of its formulation. It is possible to conduct such tests today.

Wang and Kaufman also describe in chapter 4 an extension of the MNLS to deal with incoherent sources of field power. This extension was specifically developed to permit forming images of extended sources associated with data similar to those illustrated by Fig. 1.9. Thus, it is intended to make it possible to delineate regions of cortex that become more active relative to their surroundings as well as regions whose activity is suppressed as subjects engage in various mental tasks. It seems likely that simple ECDs may not be very useful as source models when dealing with variations in alpha power. MEG studies have indicated that alpha spindles are generated by time-varying configurations of a large number of discrete sources (Ilmoniemi, Williamson, & Hostetller, 1988; Williamson, Wang, & Ilmoniemi, 1989).

As we note in the last section of this chapter (APPLICATIONS OF MSI), one of the ostensible advantages of MSI is that it is capable of re-

solving very small differences in time of onset and duration of activity of different cortical regions. Thus, when applied to studying cognitive processes it is capable of determining the temporal order of activation of these regions of cortex. When coupled with images of areas of cortical activation, this fine temporal resolution should be extraordinarily helpful in both basic and clinical research.

The Spatial Resolution of MSI

The spatial resolution of an instrument may be defined in several different ways. In the field of optics, for example, it was once defined as the minimum angular separation of pairs of points or bars that would permit them to be distinguished from a single point or bar. Thus, the older vision literature refers to the minimum detectable separation of two black bars on a white background, which is sometimes given as 1 arcmin. This measure of

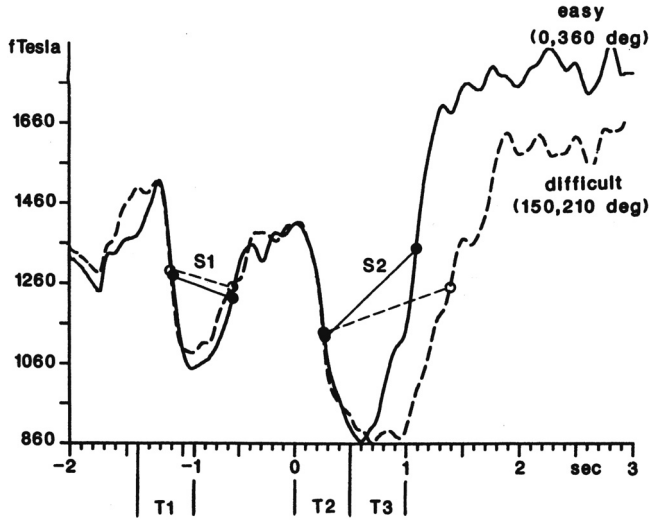

FIG. 1.9. Average variation in amplitude of alpha activity over a 5-sec epoch as the subject engages in mental rotation tasks. Alpha amplitude (in femtoTesla) is the square root of mean field power in the band of 8 Hz to 12 Hz. Time in seconds is shown along the abscissa. A letter of the alphabet was presented at Time 0, and the subject had to decide if it was the same as a previously seen upright letter (inspection letter) or its mirror image. The letter at Time 0 might be upright or tilted at an angle as well as left–right reversed. The task was more difficult for a large angle of tilt than for a small one. This is reflected in reaction time, which increased with tilt angle. The solid line represents data obtained when the task was easy (no tilt angle) and the dashed line when the task was difficult. Note that the depression in the level of alpha had the same duration (S1) for the inspection letter in both the easy and difficult tasks. However, S2 is markedly different, as it is much longer for the difficult than for the easy tasks. S2 is highly correlated with reaction time for all six subjects in this study. deg = degrees. (Adapted from Michel et al., 1993).

resolution proved to be inadequate as it could not predict the detectability of separation of spatial patterns with configurations even slightly different, for example, bars with the same spatial layout but of different contrast. Furthermore, lines, bars, dots, and letters of the alphabet all yielded seemingly incommensurable results. This ambiguity ultimately led to the development of Fourier optics and to the definition of resolution in terms of the spatial modulation transfer function which, in vision, is referred to as the *contrast sensitivity function*. In optics, linear systems analysis based on measured modulation transfer functions predicts the spatial resolution of optical systems for spatial patterns with arbitrary configurations.

The concept of *resolution* is also used to compare functional brain imaging modalities, but similar ambiguities apply here as well. In some cases resolution is defined as the minimum detectable separation of two relatively active regions of cerebral cortex. In positron emission tomography (PET) or fMRI, resolving two regions of active neural tissue is limited in part by physical properties of blood flow in and around the active tissue as well as the physical attributes of the sensor systems. For MSI, the literature sometimes reports that it provides a spatial resolution of about 1 to 2 cm (Committee on the Mathematics and Physics of Emerging Dynamic Biomedical Imaging, 1996). However, this estimate seems inconsistent with some empirical observations. This inconsistency may be due in part to the ambiguity inherent in the use of the term *resolution*. Unfortunately, as yet there have been no serious efforts to calibrate neuromagnetometers in terms of their actual abilities to resolve sources of extra-cranial magnetic fields. Instead, researchers have focused on the accuracy with which MSI can localize single sources. The accuracy of localizing a single source is affected by many factors, including (a) the signal-to-noise ratio of the MEG recording, (b) the number of and nature of spatial samples of the extracranial magnetic field, (c) the precision of location and orientation of the sensor in three-dimensional space relative to the head, (d) the depth of the source and how close the source is to the center of the best-fitting local sphere, (e) the assumed head model (see chap. 3), (f) prior knowledge of the anatomy of the surface on which the source may exist (see chap. 4), (g) approximations in computation of the forward solution (see chap. 3), and (h) the extent of and variability in the spatial distribution of the source.

Several studies (cf. Barth, Sutherling, Broffman, & Beatty, 1986; Weinberg, Brickett, Coolsma, & Baff, 1986; Yamamoto et al., 1988) have demonstrated an accuracy of ~3 mm in locating a current dipole source, provided that the signal-to-noise ratio is sufficient to permit repeated

measures and that the spatial sampling of the field is adequate to permit generating a good fit to a computed isofield contour map. These conditions occurred when the actual source was within 4 cm to 5 cm of the surface of the skull. Barth et al. (1986) found that the accuracy worsened to 8 mm to 9 mm as the source was placed at increasingly greater depths in the head. (In this experiment the source was a virtual current dipole inside a cadaver's skull filled with a conducting gel.) In all of these cases the current dipole was oriented so that it was totally or largely tangential to the overlying skull, for otherwise the strength of its radial field would have been vanishingly small (Cohen, Cuffin, Yunokuchi, Maniewski, Purcell, Cosgrove, et al., 1990; see comments by Williamson, 1991, and by Hari, Hamalainen, Ilmoniermi, & Lounasmaa, 1991).

It is particularly instructive to reconsider the experimental determination of the tonotopic map of the human auditory cortex (Romani et al., 1982). This experiment was conducted using a single-channel neuromagnetometer, but the field was sampled at a very large number of positions in many repeated trials. At each placement of the single-channel neuromagnetometer the stimulus was an amplitude-modulated sinusoidal tone of each of several different carrier frequencies ranging from 100 Hz to 4000 Hz. The isofield contour map obtained at each of these carrier frequencies was not determined until all of the data were collected and sorted by carrier frequency. It is likely that if each stimulus were a complex tone composed of several different carrier frequencies, the resulting map would have been indistinguishable from that generated by a single equivalent current dipole. Yet when the maps were based on separated sets of trials, they differed significantly from each other. In fact, on the basis of the data they obtained, Romani et al. were able to "resolve" sources separated from each other by distances of a few millimeters. Similarly, in studying the organization of the first and second somatosensory cortices, Hari et al. (1984) obtained millimeter accuracy in resolving these sources.

It should be borne in mind that if Romani et al. (1982) had presented two of their stimuli concurrently, the resulting field map is likely to have been similar to one generated by a single dipole. Hence, strictly speaking, they would have been unable to resolve the ostensibly two sources contributing to the net field. However, with precise prior knowledge of the anatomy, along with the assumption that the sources "lived" on the surface of the cortex, then the MNLS inverse—or, possibly, related methods—could have differentiated the multiple sources. Naturally, this would depend on the amount of noise in the data but, thus far, although

encouraging, studies of the effect of noise on such computations have been conducted only in computer simulations.

It is rather surprising that research has not yet been conducted using the techniques devised by Regan and Regan (chap. 5) to determine how well MSI can resolve two concurrently activated cortical areas. Consider the following hypothetical experiment: Two tones of different frequency are modulated by two harmonically unrelated low-frequency sinusoids. All of the MEG data collected at a single position are sorted so that the strength of the field fluctuating at the frequency of one of the two sinusoids is averaged separately from that of the field fluctuating at the frequency of the other sinusoid. This may result in two different field maps and permit resolution of two different sources along the surface of the auditory cortex. If the stimuli should produce effects that exhibit nonlinear interactions, then the results could not be predicted from the sum of the results obtained by presenting the two stimuli separately. Even here, however, responses at the frequencies of the sidebands may be detectable as well. In any event, we still do not fully appreciate the ability of MSI to resolve sources. Neither do we yet understand how rich the potential results of such investigations may be.

COMPLEMENTARY FUNCTIONAL IMAGING MODALITIES

In this section we briefly review several of the most widely cited forms of functional brain imaging. We do this so MSI can be seen in perspective, especially as it is now evident that these different modalities complement each other; that is, their joint use may well yield more information than can be achieved by using any method alone.

The imaging modalities we review here are primarily PET and fMRI. We touch only lightly on EEG, as it was considered extensively earlier in this chapter. We do not deal at all with electrical impedance tomography (cf. Holder, 1993), because it is not yet widely cited. Neither do we discuss single photon emission tomography, as it appears to be waning in importance as a functional imaging modality. It is important to note, however, that some efforts have been made to combine MEG with impedance tomography. The connection seems quite natural, as magnetic field sensors can be used to monitor the flow of currents imposed on the body. In chapter 11, Maclin describes PET and fMRI in some detail, as well as the newly emerging modality of optical (near infrared) spectroscopy and the related evoked optical response. In this section we deal largely with the relation among MSI, PET, and fMRI. We consider the relative advantages and disadvantages of each modality and mention some ostensible advantages associated with combining them.

PET

PET is based on detection of positron emitting radiotracers (Bohm, Eriksson, Bergstrom, Litton, & Sundman, 1987; Ter-Pogossian, Mullani, Hood, Higgins, & Ficke, 1978; Thompson, Yamamoto, & Meyer, 1979). A PET scanner detects gamma rays from intravenously administered (or inhaled) positron-emitting isotopes. Paired gamma ray detections are computed into functional images. With the radio-labeled tracers in the subject's blood, PET provides an indirect measure of neuronal activity through direct measurements of local blood flow or metabolism change as a function of task performance. In certain clinical applications the concern is with sustained metabolic levels. Deviation from normal is indicative of some disease processes.

A number of positron-emitting radiotracers can be used for PET. The most commonly used are fluorine (F18) and oxygen (O15). Fluorine is normally used to measure glucose metabolic rate. It provides a spatial resolution of about 3.5 mm in a plane but a temporal resolution of about 32 minutes. Attached to water molecules, O15 is used in PET to measure patterns of blood flow. The spatial resolution is not as good as the F18 method; however, the temporal resolution is about 60 sec.

Because fMRI offers better temporal and spatial resolution and does not require injection of radioactive materials, fMRI is preferred by many researchers. However, the diversity of specific brain chemical systems provides PET with a unique advantage over other imaging modalities. For example, PET can be used with other radiolabels (e.g., L-dopa) to image aspects of the dopamine, serotonin, benzodiazapine, N-methyl-D-aspartate, and other neurotransmitter systems.

Ingenious experiments have been performed to determine which regions of the brain become active during performance of different cognitive tasks (cf. Raichle, 1997). However, it is not possible to determine the temporal order in which these regions are activated.

fMRI

As a relative newcomer in brain imaging, fMRI is rapidly becoming the most popular functional imaging modality for basic research purposes. Many university laboratories devoted to cognitive neuroscience and psychology already have or soon will have installed powerful state-of-the-art fMRI systems. Basically, an fMRI system measures changes in blood oxygenation and blood volume correlated with neural activity (Belliveau et al., 1992; Ogawa et al, 1993; chap. 11, this volume). Consider a working model for one

of the most commonly used imaging methods in fMRI: blood oxygenation level dependent fMRI. An increase in neuronal activity causes local vasodilatation, which results in an increased local blood flow. The need for oxygenated hemoglobin generated by neural activity exceeds the need associated with the resting metabolic processes. The locally increased ratio of oxygenated hemoglobin (a diamagnetic substance with low magnetic susceptibility) and deoxygenated hemoglobin (a paramagnetic substance with high magnetic susceptibility) reduces the microscopic magnetic field in homogeneities in the neighborhood of venules, veins, and red blood cells within veins. This leads to increased image intensity in MRI.

Using strong magnetic fields and the principle of nuclear resonance, fMRI, like PET, provides an indirect measure of neuronal activity through direct measurements of local blood oxygenation level or flow as a function of task performance. At the time of this writing, the state-of-the-art fMRI systems typically provide approximately $3 \times 3 \times 4$ mm spatial resolution. The temporal resolution of fMRI, however, is on the order of seconds, limited by the slowness of the hemodynamics.

EEG

Three major advantages of EEG are (a) high temporal resolution (up to millisecond accuracy), (b) direct measurement of postsynaptic potential, and (c) relatively inexpensive instrumentation (a high-density EEG system costs about $100–200K). However, it suffers from ambiguities in source localization. The spatial resolution of EEG is estimated to be a couple of centimeters.

MEG shares the two advantages with EEG: (a) high temporal resolution and (b) direct measurement of postsynaptic potential. However, as we pointed out early in this chapter, a major additional advantage of MEG lies in the transparency of intervening tissue to magnetic fields and, consequently, much simpler magnetic inverse solutions. The spatial resolution of MEG is estimated to be 2 mm to 5 mm (a figure that depends on the depth of the source). On the other hand, MEG is about one order of magnitude more expensive than EEG.

Assuming that cortical regions involved in mental tasks can be identified, it is possible to determine the order of activation using either EEG or MEG.

Combining the Modalities

MRI as a method for imaging anatomical structures is also of great potential use, especially in identifying the structures where current dipole sources

computed from MEG and EEG data may lie. As described in chapter 4, accurate information as to the geometry of the cerebral cortex is central to achieving reasonable inverse solutions for imaging current distributions. So it is now obvious that whenever extensive EEG or MEG mapping is conducted to reveal the locations of lesions or places at which various mental processes are implemented, high-resolution MRI scans are required.

Whereas both PET and fMRI offer excellent spatial resolution (e.g., Belliveau et al., 1992; Raichle, 1997), EEG and MEG offer very good temporal resolution (e.g., Kaufman & Williamson, 1980; Regan, 1989). As a consequence, it is widely recognized that the optimal brain imaging strategy for cognitive neuroscience is a combination of different imaging modalities (Belliveau et al., 1993; Dale & Sereno, 1995; George et al., 1995; Heinze et al., 1994; Korvenoja et al., 1999; Mangun, Buonocore, Girelli, & Jha, 1998; Menon, Ford, Lim, Glover, & Pfefferbaum, 1997; Simpson et al., 1993). This includes joint spatiotemporal analyses of simultaneous recordings of two imaging modalities—for example, fMRI and EEG—as well as MRI/fMRI constrained EEG/MEG source localization.

It is important to recognize that different imaging modalities measure different physical phenomena and do not necessarily provide a direct measure of neural activity. Hence, the measures obtained using one imaging modality may not necessarily correspond to those registered by another modality. Furthermore, the spatial locations of "neural activity" registered by one modality may not be identical to that obtained via another modality (cf. chap. 11). Put more explicitly, an emerging research problem is that of determining the degree to which regions of altered blood flow are commensurate with regions of enhanced or depressed neural activity, and in identifying whether a change in blood flow represents enhancement or depression in local neural activity. The joint use of MSI and fMRI is essential to resolving this problem.

APPLICATIONS OF MSI

As described in many of the chapters of this book, MSI is widely applied in medicine; it also finds use as a basic research modality, especially in the field of cognitive neuroscience. In the 1970s, researchers working in what came to be called *biomagnetism* in general, and *neuromagnetism* in particular, focused on developing instruments with sufficient sensitivity to measure the weak fields generated by biological phenomena. Instrumentation based on advances in low-temperature physics was of primary concern, because it enabled detection of exquisitely weak magnetic fields. As this technology improved, it became possible to routinely detect and map

neuromagnetic fields. Then, in the 1980s and 1990s, the emphasis shifted to applying the technology to medicine and to cognitive science.

Most of the remaining chapters in this volume provide many instances of how MSI is and has been applied. Clinical applications to stroke and in epilepsy are described in chapters 11 and 14. The systems now being used in clinical settings are described in chapters 7 through 9. In chapter 9, Lounasmaa and Hari also describe many of the results obtained in their Helsinki laboratory that bear on cognitive science. Many other chapters also describe results related to sensory and cognitive processes. In chapter 13, Lu and Sperling examine the way in which the temporal resolution of MEG makes it possible to determine the decay times of neural processes occurring concurrently at different places in the brain. They illustrate how this may help to determine the time courses of iconic and echoic short-term memory as well as clarify the relation between different levels of processing of sensory information. Chapter 13 also contains an excellent introduction to how one might use both MSI and psychophysical strategies in examining issues of central concern to cognitive science. This is an area that is ripe for major discoveries.

REFERENCES

Barth D. S., Sutherling W., Broffman, J., & Beatty J. (1986). Magnetic localization of a dipolar current source implanted in a sphere and a human cranium. *Electroencephalography & Clinical Neurophysiology, 63,* 260–262.

Belliveau, J. W., Baker, J. R., Kwong, K. K., Rosen, B. R., George, J. S., Aine, C. J., Lewine, J. D., Sanders, J. A., Simpson, G. V., & Foxe, J. J. (1993). Functional neuroimaging combining fMRI, MEG, and EEG. *Proceedings of the International Society of Magnetic Resonance Medicine, 1*, 6.

Belliveau, J. W., Kwong, K. K., Kennedy, D. N., Baker, J. R., Stern, C. E., Benson, R., Chesler, D. A., Weisskoff, R. M., Cohen, M. S., Tootell, R. B. H., Fox, P. T., Brady, R. J., & Rosen, B. R. (1992). Magnetic Resonance Imaging Mapping of Brain Function—Human Visual Cortex. *Investigative Radiology, 27*(S2), S59–S65.

Bohm, C., Eriksson, L., Bergstrom, M., Litton, J., & Sundman, R. (1978). A computer assisted ring detector positron camera system for reconstruction tomography of the brain. *IEEE Transactions on Nuclear Science, NS, 25,* 624–636.

Brenner, D., Lipton, J., Kaufman, L., & Williamson, S. J. (1978). Somatically evoked fields of the human brain. *Science, 199*, 81.

Brenner, D., Williamson, S. J., & Kaufman, L. (1975, October). Visually evoked magnetic fields of the human brain *Science, 190,* 480–482.

Cohen, D., Cuffin, B. N., Yunokuchi, K., Maniewski, R., Purcell, C., Cosgrove, R., Ives, J., Kennedy, J. G., & Schomer, D. L. (1990). MEG versus EEG localization test using implanted sources in the human brain. *Annals of Neurology, 28,* 811–817.

Committee on the Mathematics and Physics of Emerging Dynamic Biomedical Imaging. (1996). *Mathematics and physics of emerging biomedical imaging*. National Academy Press: Washington, DC.

Curtis, S., Kaufman, L., & Williamson, S. J. (1988). Divided attention revisited: Selection based on location or pitch. In K. Atsumi, M. Kotani, S. Ueno, T. Katila, & S. J. Williamson (Eds.), *Biomagnetism, 87* (pp. 138–141). Tokyo: Denki University Press.

Dale, A. M., & Serena, M. I. (1995). Improved localization of cortical activity by combining EEG and MEG with MRI cortical surface reconstruction: A linear approach. *Journal of Cognitive Neuroscience, 5*(2), 162–176.

George, J. S., Aine, C. J., Mosher, J. C., Schmidt, D. M., Ranken, D. M., Schlitt, H. A., Wood, D. C., Lewine, J. D., Sanders, J. A., & Belliveau, J. W. (1995). Mapping function in the human brain

with magnetoencephalography, anatomical magnetic resonance imaging, and functional magnetic resonance imaging. *Journal of Clinical Neurophysiology, 12*(5), 406–431.

Hari, R., Hamalainen, M., Ilmoniemi, R., & Lounasmaa, O. V. (1991). MEG versus EEG localization test. *Annals of Neurology, 30,* 222–223.

Hari, R., Reinikaninen, K., Kaukoranta, E., Hämäläinen, M., Ilmoniemi, R., Penttinen, A., Salminen, J., & Teszner, D. (1984). Somatosensory evoked cerebral magnetic fields from SI and SII in man. *Electroencephalography & Clinical Neurophysiology, 57,* 254–263.

Heinze, H. J., Mangun, G. R., Burchert, W., Hinrichs, H., Scholz, M., Munte, T. F., Gos, A., Scherg, M., Johannes, S., Hundeshagen, H., Gazzaniga, M. S., & Hillyard, S. A. (1994). Combined spatial and temporal imaging of brain activity during visual selective attention in humans. *Nature, 372,* 543–546.

Helmholtz, H. von. (1885) *On the sensations of tone,* From 4th German ed. A. J. Ellis (Trans.), New York, Dover, 1954. (Original work published 1885)

Holder, D. (Ed.). (1993). *Clinical and physiological applications of electrical impedance tomography.* London: UCL Press Limited.

Ilmoniemi, R. J., Williamson, S. J., & Hostetler, W. E. (1988). New method for the study of spontaneous brain activity. In K. Atsumi, K. Kotani, S. Ueno, T. Katila, & S. J. Williamson (Eds.), *Biomagnetism, 87* (pp. 182–185). Tokyo: Tokyo Denki University Press.

Kaufman, L., Curtis, S., Wang, J. Z., & Williamson, S. J. (1991). Changes in cortical activity when subjects scan memory for tones. *Electroencephalography & Clinical Neurophysiology, 82,* 266–284.

Kaufman, L., Kaufman, J. H., & Wang, J. Z. (1991). On cortical folds and neuromagnetic fields. *Electroencephalography & Clinical Neurophysiology, 79,* 211–226.

Kaufman, L., & Locker, J. (1970). Sensory modulation of the EEG. *Proceedings of the 78th Annual Convention of the American Psychological Association, 1*, 79–80.

Kaufman, L., & Price, R. (1967). The detection of cortical spike activity at the human scalp. *IEEE Transactions on Bio-Medical Engineering. BME-14*, 84–90.

Kaufman, L., Schwartz, B. S., Salustri, C., & Williamson, S. J. (1990). Local inhibition of spontaneous brain activity during mental imagery. *Journal of Cognitive Neuroscience, 2,* 124–132.

Kaufman, L., & Williamson, S. J. (1980). The evoked magnetic field of the human brain. In F. L. Denmark (Ed.), *Psychology: The leading edge.* New York: New York Academy of Sciences, 45–65.

Korvenoja, A., Huttunen, J., Salli, E., Pohjonen, H., Martinkauppi, S., Palva, L. M., Lauronen, L., Virtanen, J., Ilmoniemi, R. J., & Aronen, H. J. (1999). Activation of multiple cortical areas in response to somatosensory stimulation: Combined magnetoencephalographic and functional magnetic resonance imaging. *Human Brain Mapping, 8*, 13–27.

Liegeois-Chauvel, C., Giraud, K., Badier, J.-M., & Marquis, P. (2001). Intracerebral evoked potentials in pitch perception reveal a functional asymmetry of the human auditory cortex. In R. J. Zatorre & I. Peretz (Eds.), *The biological foundations of music*. New York: New York Academy of Sciences.

Lu, Z.-L., & Williamson, S. J. (1991). Spatial extent of coherent sensory-evoked cortical activity. *Experimental Brain Research, 84,* 411–416.

Mangun, G. R., Buonocore, M. H., Girelli, M., & Jha, A. P. (1998). ERP and fMRI measures of visual spatial selective attention. *Human Brain Mapping, 6,* 383–389.

Menon, V., Ford, J. M., Lim, K. O., Glover, G. H., & Pfefferbaum, A. (1997). Combined event-related fMRI and EEG evidence for temporal-parietal cortex activation during target detection. *Neuroreport, 8,* 3029–3037.

Michel, C., Kaufman, L., & Williamson, S. J. (1993). Duration of EEG and MEG alpha suppression increases with angle in a mental rotation task, *Journal of Cognitive Neuroscience, 6*(2), 139–150.

Nunez, P. L. (1981). *Electric fields of the brain: The neurophysics of EEG*. New York: Oxford University Press.

Ogawa, S., Menon, R. S., Tank, D. W., Kim, S.-G., Merkle, H., Ellermann, J. M., & Ugurbil, K. (1993). Functional brain mapping by blood oxygenation level-dependent contrast magnetic resonance imaging: A comparison of signal characteristics with a biophysical model. *Biophysics Journal, 64,* 803–812.

Ottaviani, F., Di Girolamo, S., Briglia, G., De Rossi, G., Di Giuda, D., & Di Nardo, W. (1997, September–October). Tonotopic organization of human auditory cortex analyzed by SPECT. *Audiology, 36,* 241–248.

Raichle, M. E. (1997). Functional brain imaging and verbal behavior. In J. W. Donahoe & V. P. Dorsel (Eds.), *Neural-network models of cognition: Biobehavioral foundations* (pp. 438–454). Amsterdam: North-Holland/Elsevier Science.

Regan, D. (1989). *Human brain electrophysiology: Evoked potentials and evoked magnetic fields in science and medicine*. New York: Elsevier.

Regan, D., & Regan, M. P. (1987). Nonlinearity in human visual responses and a limitation of Fourier methods. *Vision Research, 27,* 2181–2183.

Rojas, D. C., Teale, P. D., Sheeder, J. L., & Reite, M. L. (2000). Neuromagnetic alpha suppression during an auditory Sternberg task. Evidence for a serial, self-terminating search of short-term memory. *Cognitive Brain Research, 10,* 85–89.

Romani, G. J., Williamson, S. J., & Kaufman, L. (1982, June). Tonotopic organization of the human auditory cortex. *Science, 216,* 1339–1340.

Simpson, G. V., Pflieger, M. E., Foxe, J. L., Ahlfors, S. P., Vaughan, H. G., Hrabe, J., Ilmoniemi, R. J., & Lantos, G. (1995). Dynamic neuroimaging of brain function. *Journal of Clinical Neurophysiology, 12*(5), 432–449.

Ter-Pogossian, M. M., Mullani, N. A., Hood, J. T., Higgins, C. S., & Ficke, D. C., (1978). Design considerations for a positron emission transverse tomograph (PETT V) for imaging of the brain. *Journal of Computer Assisted Tomography, 2,* 539–544.

Thompson, C. J., Yamamoto, Y. L., & Meyer, E. (1979). Positome II: A high efficiency positron imaging device for dynamic brain studies. *IEEE Transactions on Nuclear Science, NS, 26,* 583–389.

Weinberg, H., Brickett, P., Coolsma, F., & Baff, M. (1986). Magnetic localization of intracranial dipoles: Simulation with a physical model. *Electroencephalography & Clinical Neurophysiology, 64,* 159–170.

Wessinger, M. C., Buonocore, M. H., Kussmaul, C. L., & Mangun, G. R. (1997). Tonotopy in human auditory cortex examined with functional magnetic resonance imaging. *Human Brain Mapping, 5,* 18–25.

Williamson, S. J. (1991). MEG versus EEG localization test. *Annals of Neurology, 30,* 222–222.

Williamson, S. J., Wang, J. Z., & Ilmoniemi, R. (1989). Method for locating sources of human alpha activity. In S. J. Williamson, M. Hoke, G. Stroink, & M. Kotani (Eds.), *Advances in biomagnetism* (pp. 257–260). New York: Plenum.

Yamamoto, T., Williamson, S. J., Kaufman, L., Nicholson, C., & Llinas, R. (1988). Magnetic localization of neuronal activity in the human brain. *Proceedings of the National Academy of Sciences (USA), 85,* 8732–8736.